Materials Research. 2024; 27:e20240235
DOI: https://doi.org/10.1590/1980-5373-MR-2024-0235

Bioactive TiO_2 Fibers Prepared by Solution Blow Spinning: A Promising Approach for Microbial Control

Tiago Cesar Gimenes[a], Guilherme Schiavão Padovani[a], Eloisa Aparecida Carvalho Silva[a], Higor de Souza Silva[a], Gabriel Menegolo De Castro Meira[a], Alex Otávio Sanches[a], José Antônio Malmonge[a], Alexandre J. Gualdi[b], Fernando R. de Paula[a*]

[a]*Universidade Estadual Paulista (UNESP), Faculdade de Engenharia, Ilha Solteira, SP, Brasil.*
[b]*Universidade Federal de São Carlos (UFSCar), 13565-905, São Carlos, SP, Brasil.*

Received: May 22, 2024; Revised: July 26, 2024; Accepted: August 01, 2024

PEO/TiP fibers were obtained using the Solution Blow Spinning (SBS) apparatus and heat treated to produce TiO_2 fibers. The morphological and structural characteristics were assessed using SEM and X-ray diffraction. The fibers, with a thickness of 12 µm, showed a change in crystalline structure with heat treatment. At temperatures as low as 800 °C, only the anatase phase was identified, while at 900 °C, both anatase and rutile phases coexisted. The addition of TiP to the polymer matrix reduced the initial breakdown temperature, and the DSC curves showed exothermic peaks due to the amorphous phase transition to TiO_2/anatase. The fibers' photocatalytic capacity was tested, revealing that TiO_2-fibers in the anatase phase achieved 97% degradation of Rhodamine-B dye in 40 minutes. The study found that the biocide efficacy of TiO_2-fibers depends on their heat treatment. Fibers with anatase/rutile or pure rutile phases did not show significant efficiency. However, fibers treated at 600°C with pure anatase phase were more effective in eliminating E. coli and total coliforms. Finally, we can state that the TiO_2 fibers obtained in this work using the SBS technique can be used to produce filters to purify water contaminated by pathogens dangerous to human health or even to purify the air.

Keywords: *TiO_2 fibers, solution blow spinning, photocatalytic property, PEO/TiP.*

1. Introduction

Photocatalysis has emerged as a promising technology for degrading organic pollutants, dyes, and antibacterial applications[1-4]. Currently, this technology is widely used in water treatment[5-8]. Several broadband semiconductors, such as TiO_2[9], WO_3[10], Cu_2O[11], and CdS[12] have been employed in photocatalytic processes to achieve this goal. In semiconductors TiO_2[13-18] is widely used due to its environmental friendliness, high removal rate[9], low toxicity, low cost[19], and high photocatalytic activity[20]. Photocatalytic fiber semiconductors have recently been used for wastewater treatment due to their adjustable pore architectures, huge specific surface areas, and nanoscale and micrometer diameters[21-27]. Fibers may be created using various techniques, including electrospinning, phase separation, self-assembly, and stretching[28,29].

Electrospinning is a well-established technique for polymeric production of fibers from melt polymers or polymer solutions[25,30-32]. The method depends on the polymer solution's dielectric properties and high-voltage electric field to produce the polymer fibers.

The amount of "free" charge that can be induced in a polymer solution during electrospinning is represented by the dielectric constant of the solvent. Low dielectric constant polymer-solvent solutions limit the initiation of the whipping instability and thinning of the polymer jet[33,34]. Because of these constraints, the SBS technique has recently been highlighted in producing polymeric micro/nanfibers[35-41].

Compared with electrospinning, the SBS process does not depend on the dielectric constant; fibers can be deposited onto any type of substrate or collector, and the fiber production rate is many times higher, thus having better commercial production potential[35]. As a result, this study aimed to create TiO_2 photocatalytic microfibers by thermally treating polyethylene oxide/isopropoxide (PEO/TiP) fibers generated by the SBS apparatus. The influence of thermal treatment on the morphology and crystalline structure of TiO_2 microfibers was examined first, followed by an assessment of the photocatalytic activity of microfibers as function of the degradation of the Rhodamine-B (RhB) dye under UV light. The efficiency of TiO_2 fibers in the death of bacteria such as E. coli and total coliforms was also evaluated. The results of this study can provide valuable information on the use of TiO_2 fibers in various applications, such as water treatment contaminated with pathogens harmful to human health and air purification by pathogens harmful to human health and air purification.

*e-mail: fernando.r.paula@.unesp.br

2. Experimental Procedure

2.1. Materials

All chemicals used in this work were purchased from Sigma-Aldrich and used as received: polyethylene oxide powder (PEO) (Average Mw = 5,000,000) titanium (IV) isopropoxide (TiP) (≥ 95.0%), RhB dye (≥ 95.0%), chloroform (≥ 99.5%), and absolute ethanol (≥ 95.0%).

2.2. Extraction of pure titanium dioxide fibers

The precursor solution was prepared by adding 0.2 g of PEO to a mixture of 3.0 mL of absolute ethyl alcohol and 5.0 mL of chloroform. The mixture was stirred for 40 minutes at room temperature (25 °C). Then, 2.0 mL of TiP was added to the PEO solution which remained stirred for 40 minutes. The final solution was placed in disposable syringes connected to an 18G spinal needle and attached to the injection system (Figure 1). The most optimal conditions for forming of the microfiber were as follows: injection rate of 0.3 L min^{-1}, work distance of 35 cm, and collector speed of 60 rpm. No gas was used to draw the solution to the collector. The (PEO/TiP) fibrous composites were thermally treated at 600, 700, 800, 900, and 1000 °C to remove the polymer component to yield TiO_2 fibers.

2.3. Characterization

The crystallinity and phase of the produced TiO_2 fibers were investigated using a Shimadzu X-ray diffractometer (model XRD-6000), Cu Kα (1.54056 Å). The Scherrer equation and the X-ray diffraction pattern were used to calculate the average crystallite size. A scanning electron microscope (SEM, Zeiss EVO LS15) with a voltage range of 5.00 kV to 20.00 kV was used to investigate the morphological structure. Using the image analysis tool "Image J 1.45," the average diameter of the fibers was estimated. Ten milligrams of the sample were used for the thermogravimetric analysis, which was carried out using an SDT model Q 600 from TA instruments. The samples were heated between 25 and 800 °C at 10 °C min^{-1} in a nitrogen environment with a flow rate of 100 mL min^{-1}. The Varian Cary 50 Scan equipment captured UV-vis spectra to examine the peak decrease in maximum dye absorption.

2.4. Photocatalytic principles and activity evaluation

The band gap, which forms the foundation for heterogeneous photocatalysis, is the area between the semiconductor material's valence (VB) and conduction (CB) bands. Semiconductor activation may occur depending on the energy of the photons from artificial or natural light. According to Equation 1, an electron is promoted from VB to CB by absorption of a photon with energy larger than or equal to the band gap, causing a vacancy (h+) to form in the VB. The positive potential of these vacancies might range from (+2.0 to +3.5 eV) depending on the semiconductor[42]. Figure 2 depicts a diagram showing how UV light activates TiO2 microfibers so that they can interact with contaminants such as RhB.

In the photocatalysis process, contaminants can be degraded when water molecules adsorbed on the surface of the semiconductor generate OH radicals (Equations 2 and 3)[43,44]. In addition to the OH radicals, the degradation can also occur through oxygen derivatives that are formed when electrons are captured in the system (Equation 4)[44].

$$TiO_2 \xrightarrow{h\nu} TiO_2\left(e_{CB}^{-} + h_{VB}^{+}\right) \quad (1)$$

$$h^{+} + H_2O_{adsorption} \rightarrow HO^{\cdot} + H^{+} \quad (2)$$

$$h^{+} + OH_{adsorption}^{-} \rightarrow HO^{\cdot} \quad (3)$$

$$e^{-} + O_2 \rightarrow O_2^{\cdot-} \quad (4)$$

In the development of this work, the photocatalytic activity of samples was evaluated in a photocatalytic reactor equipped with a UV mercury lamp (250 W) and a magnetic stirrer. For this purpose, 80 mg of TiO_2 fibers were added to 100 mL of RhB aqueous solution (10 mg/L). The mixture was stirred for 15 minutes at room temperature (25°C) in the absence of light. To start the photocatalysis process, the UV light was turned on, and every 10 minutes, 3 mL aliquot of the mixture was removed and then centrifuged at 6,000 RPM for 5 minutes to separate the microfibers from the solution. After this process, the solution was analyzed by

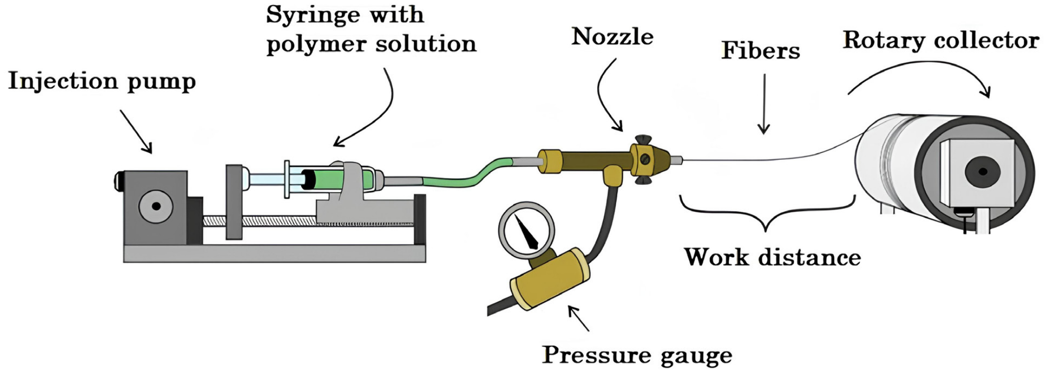

Figure 1. Experimental apparatus used by the SBS.

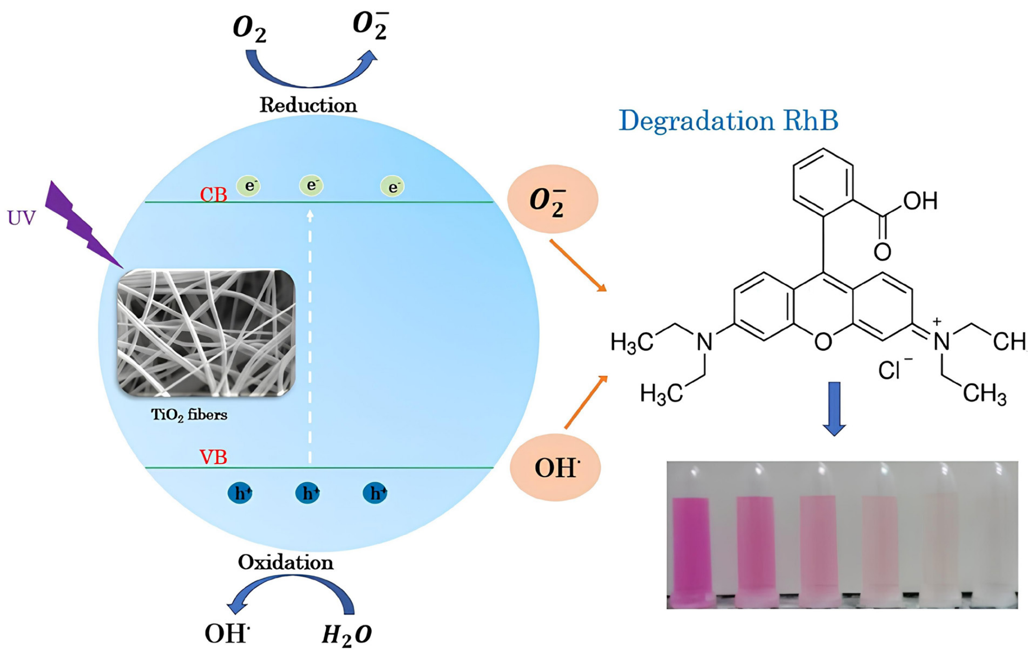

Figure 2. Photocatalytic activity of TiO_2 fibers in the presence of UV light in the RhB dye degradation process.

spectra UV-Vis, obtaining its absorption band and possible intensity reduction again.

The photocatalytic degradation efficiencies of samples were determined using the Equation 5

$$\text{Degradation}(\%) = \frac{C_0 - C}{C_0} \times 100 \tag{5}$$

where C_0 is the concentration of RhB after 15 minutes of agitation without UV exposure, and C is the RhB concentration after UV irradiation for a specific time.

2.5. Procedure for analyzing water contamination and the biocidal efficacy of TiO_2 fibers

Water samples were collected from a semi-artesian well contaminated with E. coli and total coliforms. The aim was to evaluate whether TiO_2 fibers could eliminate these bacteria. The water samples were filtered through a sterile nitrocellulose membrane with a diameter of 47 mm and a porous size of 1.45 µm to analyze the biological contaminants. This filter is designed to retain and encourage the growth of both bacteria types, E. coli (blue dots) and total coliforms (red dots) (see Figure 3a). To compare the effectiveness of TiO_2 fibers, an equivalent amount of fibers, 0,01 g, was applied to the central region of the contaminated membranes (see Figure 3b). All contaminated membranes were then exposed to a 9 W ultraviolet lamp positioned 30 cm away for a brief 2-second irradiation period. After exposure, the membranes were incubated at 36 °C for 28 hours to allow any bacterial growth. Finally, the bacterial colony formation procedure was used to evaluate qualitatively both the treated and untreated membranes, revealing the impact of the TiO_2 fibers.

3. Results and Discussion

3.1. TiO_2 fibers morphology characterization

PEO/TiO_2 fibers were produced using a blow spinning apparatus. The precise combination of injection rate, collector rotation, and working distance made producing precursor fibers without carrier gas possible. These parameters are injection rate of 53 µL, collector rotation of 60 rpm, and working distance of 35 cm. The injected PEO/TiO_2 solution presented the shape of a continuous thread that was manually taken from the tip of the nozzle to the collector, and then the rotating collector promoted the process of stretching the polymeric solution.

Figure 4 shows a SEM image of PEO/TiO_2 fibers and TiO_2 fibers resulting from the calcination of PEO/TIP at 600 °C. Fiber diameters were measured by analyzing SEM images and using ImageJ software. The distribution histograms and the calculated average diameters are shown inset in the figures. The diameter of the precursor fibers (Figure 4a) is larger than that of the calcined fibers (Figure 4b). This occurs due to the decomposition of the PEO polymer matrix. Heat treatment simultaneously removes organic components while promoting the growth of TiO_2 crystals due to oxidation of the Ti precursor.

A similar decrease in fiber diameter was also observed by Tan et al.[45], who prepared TiO_2 fibers using the SBS technique with Polyvinylpyrrolidone (PVP)/TiP. However, unlike the results shown in Figure 4, the fibers obtained after heat treatment were brittle and had reduced length compared to untreated fibers.

Figure 5 demonstrates the impact of varying temperatures on TiO_2 fibers during the heat treatment. Despite temperature changes, the fibers maintained their original form.

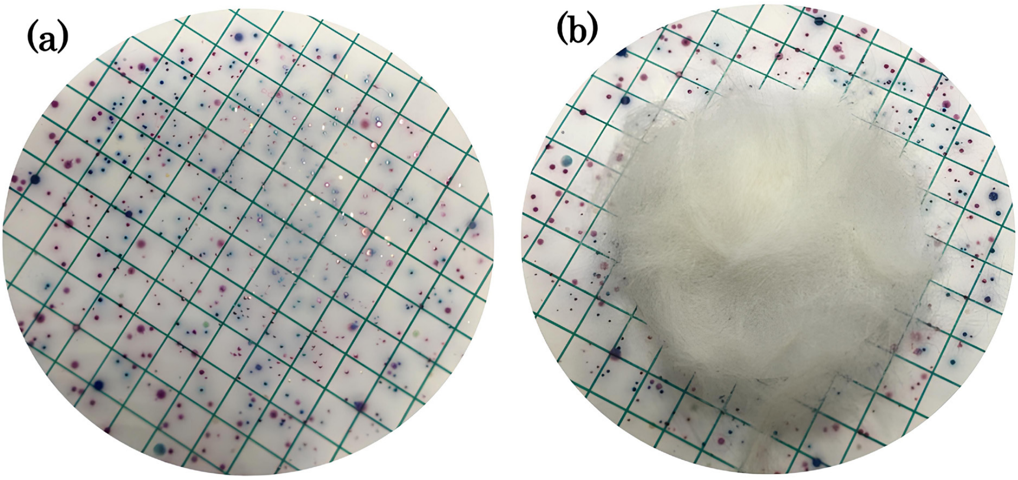

Figure 3. (a) Nitrocellulose membrane contaminated with both E. Coli (blue dots) and total coliforms (red dots) bacteria's and, (b) contaminated membrane with the presence of TiO_2 fibers.

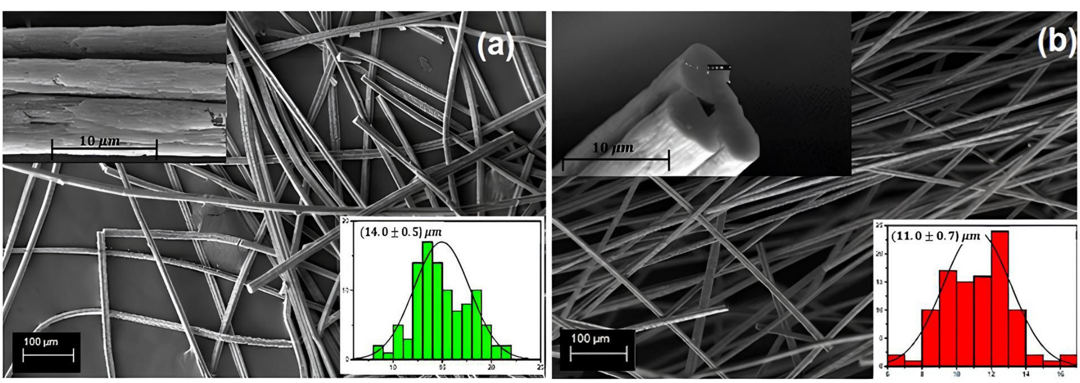

Figure 4. SEM images of PEO/TiO_2 precursor fiber (a) and (b) after heat treatment at 600 °C.

The production method allowed the development of some hollow structures, as shown in Figures 4b and 5d. It is evident from a comparison of Figures 4 and 5 that the adherence of fibers during the sintering process may cause this morphological shape. The presence of these hollow structures presents significant advantages, as it significantly increases the accessible surface area of the system, making it ideal for photocatalytic applications.

Fibers processed with SBS showed an average diameter of 11 to 13 μm after heat treatment. This draws attention to a crucial difference between electrospinning and SBS. Electrospinning best produces nanofiber architectures, while SBS generally results in fibers with substantially larger diameters. Daristotle et al.[46] who investigated the morphological and mechanical characteristics of fibers made with SBS, support this observation.

3.2. Structural analysis

The X-ray diffraction (XRD) pattern of TiO_2 fibers is depicted in Figure 6. The process of heat treatment has a significant effect on the formation of crystallographic phases. The peaks of the anatase phase are observed in the thermally treated fibers at 600, 700, and 800°C (main peak is at $2\theta = 25.3°$). In contrast, the rutile phase peaks are identified in the fibers treated at 900 and 1000 °C (main peak is at $2\theta = 27.3°$). These findings are consistent with the results reported in the literature that demonstrate using heat treatment temperatures to produce the TiO_2 phase[47,48].

To completely transform the TiO_2 fibers from the anatase phase into rutile, heat treatment at 1000 °C was necessary in this study. Usually, anatase permanently transforms into rutile when exposed to temperatures above 600 °C in an atmosphere of air. However, the transition temperature from the anatase phase to the rutile phase can vary from 400-1200 °C depending on the specific TiO_2 synthesis technique[49,50]. It is essential to evaluate the transition kinetics of these phases. Factors that should be considered include the shape and size of particles, atmosphere, surface area, sample volume, heating rate, sample container type, contaminants, and measurement technique[49].

The coexistence of anatase and rutile phases is observed in fibers treated at 900 °C. The fraction of anatase and rutile

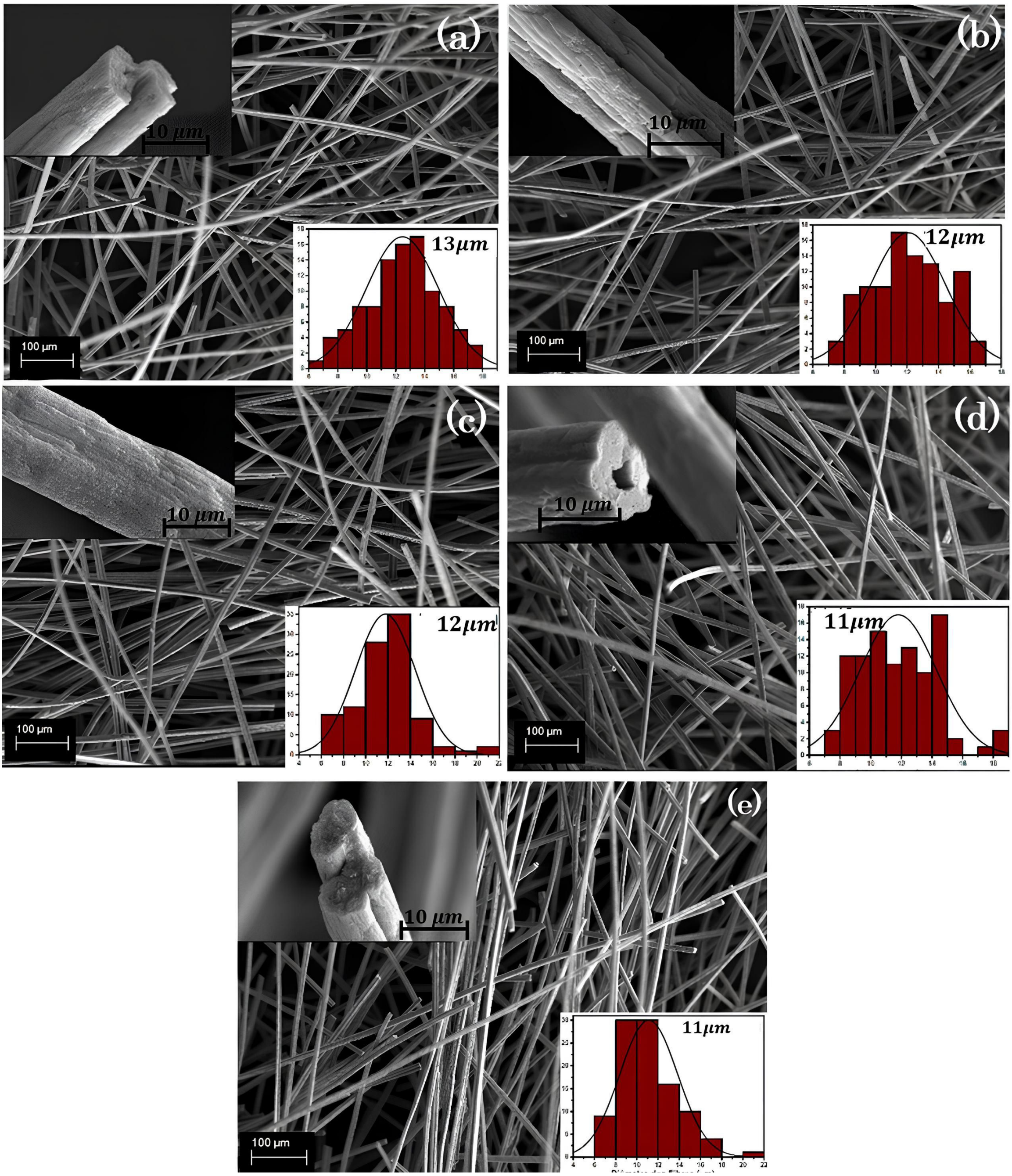

Figure 5. SEM images of TiO_2 fiber after heat treatment for 4h: (a) 600°C; (b) 700°C; (c) 800°C; (d) 900°C, and (e) 1000°C.

phases found in TiO_2 fibers was calculated using Equation 6. The rutile and anatase phases present percentages of 64.36% and 35.64%, respectively. Table 1 presents the samples' average size of the TiO_2 crystallite calculated by the Scherrer equation and the percentages of anatase and rutile phases[51,52].

$$w_R = \frac{I_R}{0{,}884 I_A + I_R}, \tag{6}$$

where W_R is the percentage of the rutile phase present in the sample, and I_R and I_A represent the intensities of the diffraction peaks characteristic of the rutile and anatase phases.

3.3. Thermal characterization

The thermogravimetric analysis (TGA) technique was utilized to gather information about the thermal stability and breakdown of the polymeric matrix of the PEO and the impact of TiP on the degradation process of the polymeric matrix. The TGA curves for pure PEO and PEO/TiP fibers are displayed in Figure 7a. A single event of mass loss was observed in the polymeric matrix (PEO), which started at around 327 °C, and the intensity decreased at approximately 405 °C, decomposing about 92% of the sample. After this event, the process continued steadily until it reached the end temperature of 800 °C. The stability of the sample is mainly due to the test being conducted in an inert atmosphere (nitrogen flow)[53].

The main byproducts of PEO mass loss are methyl alcohol, ethyl alcohol, alkene, formaldehyde, non-cyclic ethers, ethylene oxide, water, acetic aldehyde, CO_2, and CO[54,55]. In the case of the PEO/TiP composite, the integration of the precursor resulted in a decrease in the initial temperature of the polymer matrix breakdown process. There are two distinct events observed in this composite between the temperature range of 24 °C to 116 °C, with a mass loss of approximately 8%, which is attributed to ethanol and water evaporation[56]. The second event occurs between the temperature range of 197 °C to 327 °C, which is attributed to TIP decomposition and PEO degradation.

Figure 7b shows the DSC curves of the PEO matrix and PEO/TiP composite. The melting temperature of the polymer matrix (PEO) corresponds to an endothermic peak at 73 °C, while the decomposition of PEO[54] produces an endothermic peak at 380 °C. The PEO/TiP composite DSC curve shows an endothermic peak between 24 °C and 116 °C. This weight loss is due to the evaporation of water and organic solvents[57]. The exothermic peaks at 305 °C and 498 °C are due to the phase transition from amorphous to anatase TiO_2[58].

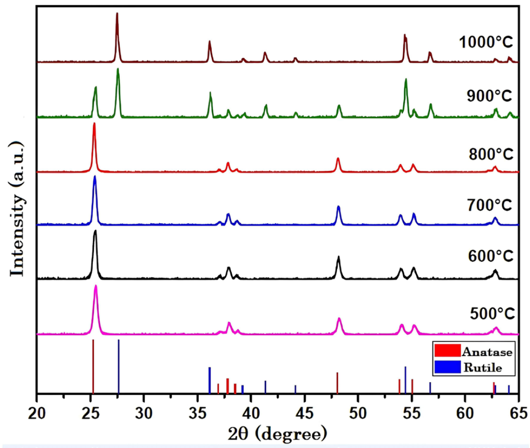

Figure 6. TiO_2 fibers XRD heat treated at different temperatures for 4 h.

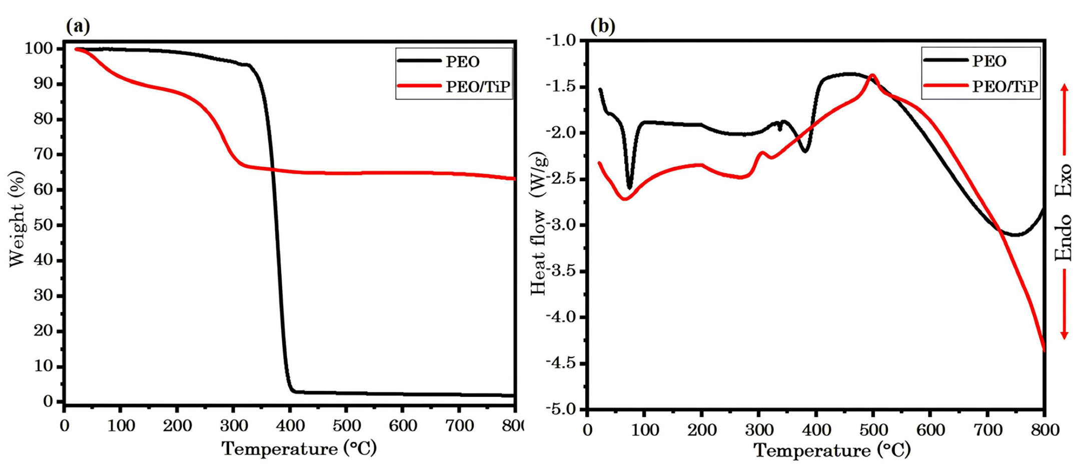

Figure 7. (a) TGA and (b) DSC curves for PEO and PEO/TiP fibers.

Table 1. Percentage of anatase and rutile phases of TiO_2 fibers submitted to different heat treatments.

Heat treatment (°C)	Percentage of phases (%)		Average crystallite size (nm)	
Temperature	Anatase	Rutile	Anatase	Rutile
600	100	0	25.26	---
700	100	0	30.63	---
800	100	0	36.73	---
900	35.64	64.36	26.24	29.18
1000	0	100	---	46.86

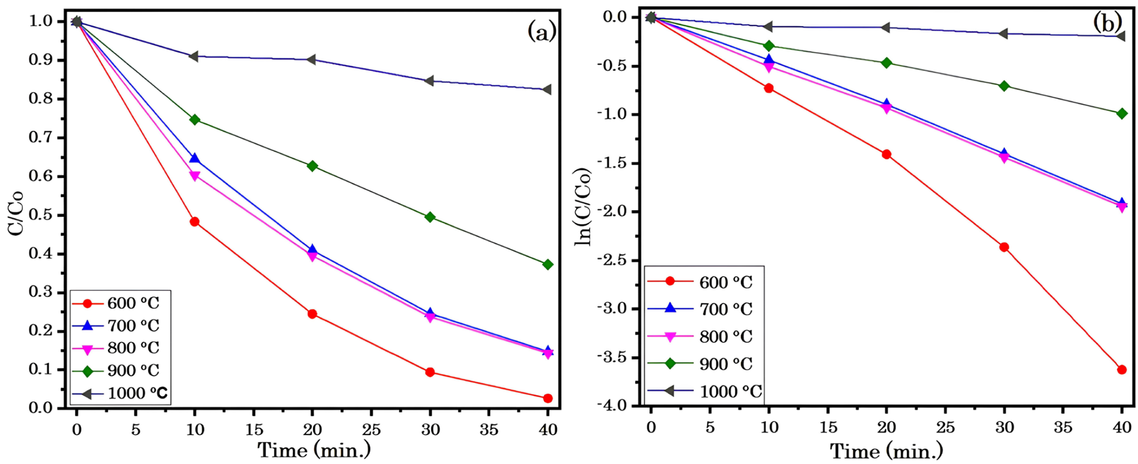

Figure 8. (a) Photodegradation of RhB by TiO_2 fibers and (b) First order kinetic model for photodegradation of RhB by TiO_2 fibers.

Table 2. RhB degradation constant by TiO_2 fibers.

Heat treatment (°C)	K (min^{-1})	R^2
600	0.0888	0.9763
700	0.0479	0.9982
800	0.0482	0.9988
900	0.0238	0.9922
1000	0.0045	0.9134

3.4. Photocatalytic performance

Figure 8 shows first-order photodegradation and kinetic graphs for TiO_2 fibers exposed to UV light (a-b). Table 2 presents the values of the degradation rate constant k (min^{-1}) for each sample. As shown in Figure 8a, after 40 minutes of reaction, the degradation of the RhB dye was 100%, 83%, 83%, 60%, and 18% for fibers heat treated at 600, 700, 800, 900, and 1000 °C, respectively. The anatase phase was the only phase present in fibers heat-treated between 600 °C and 800 °C; however, it was observed that the photocatalytic activity decreased when fibers were treated at temperatures above 600 °C. The observed decrease in photocatalytic activity is attributed to a reduction in the surface area of crystallites caused by an increase in microfiber treatment temperature. Larger average crystallite sizes correspond to a smaller surface area, resulting in a diminished number of active sites available for photocatalytic reactions (Table 1)[59-62].

It was found that for samples heat-treated at 900 °C and 1000 °C, the increase in rutile phase reduced the photocatalytic efficiency (Fig. 8a-b). The XRD patterns of TiO_2 fibers (Table 1) show increased rutile phase formation after heat treatment at higher temperatures, confirming this observation. The anatase phase generally has more significant photocatalytic activity than the pure rutile phase[63]. It is believed that the anatase phase has improved characteristics due to a decreased rate of electron-hole recombination and a stronger adsorption affinity for organic molecules[64]. However, combining different phases has been found to increase the efficiency of photocatalysis. Although some samples heated to 900 °C showed the coexistence of phases, it cannot be assumed that a heterojunction occurred in the photocatalyst, which is a fundamental factor for increased photocatalysis. Therefore, evaluating the photocatalytic activity based solely on phase composition is misleading.

3.5. Antimicrobial activity of PVDF/TiO_2 fibers

The process of photocatalytic inactivation of bacteria through TiO_2 fibers obtained at different treatment temperatures is illustrated in Figure 9. When contaminated water comes into contact with TiO_2 fibers on the surface of the membrane, ultraviolet light generates electron-hole pairs and radicals free (•OH). The •OH radical is a potent toxin capable of killing bacteria. The formation of the O_2 radical can also cause an attack, but the •OH radical is the most reactive because it can oxidize many types of organic compounds, including microbial cells. A thymine dimer forms in the bacterial DNA chromosome when the •OH radical comes into contact with the bacterial cell wall. This dimer forms knots between thymine and the DNA base, obstructing double helix formation and interrupting normal DNA replication. As a result, the cell's blocked growth eventually leads to its death. After two seconds of exposure to UV light, the TiO_2 fibers positioned in the central region of the nitrocellulose membranes significantly reduced the number of bacteria, E. coli and total coliforms, as demonstrated in Figure 9. According to the experiment, the membrane containing TiO_2 fibers in the anatase phase subjected to heat treatment at 600 °C proved to be the most effective in eliminating bacteria. The experiment results confirmed that the bactericidal efficiency of TiO_2 fibers decreases as the heat treatment temperature increases. This decrease in efficiency is due to the increase in the rutile phase, which is less effective in eliminating bacteria. It is worth mentioning that, as shown in Figure 9, the incidence time of the ultraviolet rays used in the development of the work is insufficient to kill bacteria in places without a photocatalyst. Therefore, the presence of TiO_2 fibers activated by UV radiation is responsible for the bactericidal effect.

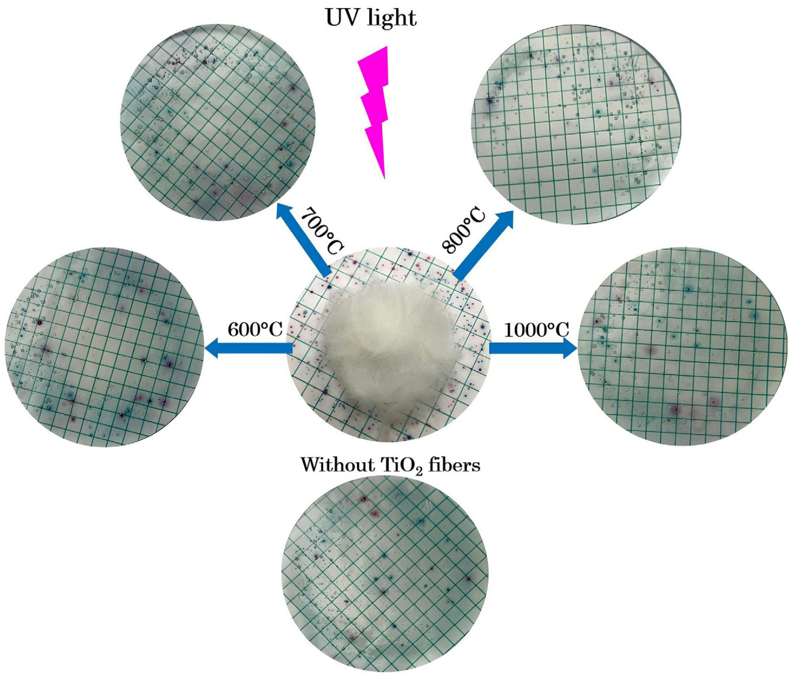

Figure 9. Sterilization efficiency results obtained for TiO_2 fibers thermally treated at different temperatures (600, 700, 800, 900 and 1000 °C) and exposed to UV radiation for 2 seconds.

4. Conclusion

In conclusion, this study demonstrates a successful method for producing PEO/Tip precursor fibers using the SBS technique without the need for pressurized gas. The best result was obtained with the sample calcined at 600 °C, which presented an anatase phase with a smaller crystallite size. With this sample, 97% of the RhB dye (aqueous solution) was eliminated after 40 minutes of exposure to UV light. According to the study involving the bactericidal activity of TiO_2 fibers, the membrane containing TiO_2 fibers in the anatase phase and treated at 600 °C was also considered the most effective for killing bacteria such as E. coli and coliforms. However, the bactericidal efficiency and photocatalytic efficiency of TiO_2 fibers decreased as the heat treatment temperature increased due to the increase in the less effective rutile phase. The results obtained in this work indicate that TiO_2 fibers produced with SBS technology have antibacterial properties, making them potential candidates for water purification applications contaminated with pathogens dangerous to human health.

5. Acknowledgments

The authors express their gratitude to São Paulo Research Foundation (FAPESP) for their financial support.

6. References

1. Baibara OE, Radchenko MV, Karpyna VA, Ievtushenko AI. A review of the some aspects for the development of ZnO based photocatalysts for a variety of applications. Physics and Chemistry of Solid State. 2021;22(3):585-94.
2. Shan D, Zhao Y, Liu L, Linghu X, Shu Y, Liu W, et al. Chemical synthesis of silver/titanium dioxide nanoheteroparticles for eradicating pathogenic bacteria and photocatalytically degrading organic dyes in wastewater. Environ Technol Innov. 2023;30:103059.
3. Zhang D, Hu H, an Wei J, Xu X, Chen L, Wu X, et al. Zr-doped TiO2 ceramic nanofibrous membranes for enhancing photocatalytic organic pollutants degradation and antibacterial activity. Colloids Surf A Physicochem Eng Asp. 2023;665:131231.
4. Ramos PG, Rivera H, Sánchez LA, Quintana ME, Rodriguez JM. Graphene-based semiconductors for photocatalytic degradation of organic dye from wastewater: a comprehensive review. Water Air Soil Pollut. 2024;235(5):292.
5. Molinari R, Lavorato C, Argurio P. Recent progress of photocatalytic membrane reactors in water treatment and in synthesis of organic compounds: a review. Catal Today. 2017;281:144-64.
6. Alswat AA, Ahmad MB, Hussein MZ, Ibrahim NA, Saleh TA. Copper oxide nanoparticles-loaded zeolite and its characteristics and antibacterial activities. J Mater Sci Technol. 2017;33(8):889-96.
7. Luong NT, Hanna K, Boily JF. Water film-mediated photocatalytic oxidation of oxalate on TiO2. J Catal. 2024;432:115425.
8. Chen L, Xu P, Zhang Y, Betts D, Ghurye GL, Wang H. Au-TiO2 nanoparticles enabled catalytic treatment of oil and gas produced water in slurry and vacuum membrane distillation systems. J Water Process Eng. 2024;65:105745.
9. Zhou Q, Zhao D, Sun Y, Sheng X, Zhao J, Guo J, et al. g–C3N4– and polyaniline-co-modified TiO2 nanotube arrays for significantly enhanced photocatalytic degradation of tetrabromobisphenol A under visible light. Chemosphere. 2020;252:126468.
10. Yang J, Xiao J, Cao H, Guo Z, Rabeah J, Brückner A, et al. The role of ozone and influence of band structure in WO3 photocatalysis and ozone integrated process for pharmaceutical wastewater treatment. J Hazard Mater. 2018;360:481-9.

11. Jiang X, Li Z, Lin Q, Dong K, Zhang Y, Sun Z. Structure, optical properties and photocatalysis performance of Cu2O microspheres prepared by hydrothermal method. J Mater Sci Mater Electron. 2016;27(8):8856-61.
12. Zhang M, Xu Y, Gong Z, Tao J, Sun Z, Lv J, et al. Enhanced charge collection and photocatalysis performance of CdS and PbS nanoclusters co-sensitized TiO2 porous film. J Alloys Compd. 2015;649:190-5.
13. Abd Aziz A, Khatun F, Uddin Monir M, Lan Ching S, Kah Hon L. TiO $_2$: a semiconductor photocatalyst. In: Ali HM, editor. Titanium Dioxide: advances and applications. London: IntechOpen; 2022. p. 1-16.
14. Dharma HNC, Jaafar J, Widiastuti N, Matsuyama H, Rajabsadeh S, Othman MHD, et al. A review of Titanium Dioxide (TiO2)-based photocatalyst for oilfield-produced water treatment. Membranes (Basel). 2022;12(3):345.
15. Anucha CB, Altin I, Bacaksiz E, Stathopoulos VN. Titanium dioxide (TiO_2)-based photocatalyst materials activity enhancement for contaminants of emerging concern (CECs) degradation: in the light of modification strategies. Chemical Engineering Journal Advances. 2022;10:100262.
16. Anucha CB, Altin I, Bacaksiz E, Stathopoulos VN. Titanium dioxide (TiO_2)-based photocatalyst materials activity enhancement for contaminants of emerging concern (CECs) degradation: in the light of modification strategies. Chemical Engineering Journal Advances. 2022;10:100262.
17. Baig N, Kammakakam I, Falath W. Nanomaterials: a review of synthesis methods, properties, recent progress, and challenges. Mater Adv. 2021;2(6):1821-71.
18. Ali S, Ismail PM, Khan M, Dang A, Ali S, Zada A, et al. Charge transfer in TiO $_2$ -based photocatalysis: fundamental mechanisms to material strategies. Nanoscale. 2024;16(9):4352-77.
19. Buama S, Junsukhon A, Ngaotrakanwiwat P, Rangsunvigit P. Validation of energy storage of TiO 2 NiO/TiO 2 film by electrochemical process and photocatalytic activity. Chem Eng J. 2017;309:866-72.
20. Cha BJ, Woo TG, Park EJ, Kim IH, An JE, Seo HO, et al. Photo-catalytic activity of hydrophilic-modified TiO 2 for the decomposition of methylene blue and phenol. Curr Appl Phys. 2017;17(11):1557-63.
21. Choi DY, Hwang CH, Lee JW, Lee IH, Oh IH, Park JY. Characterization of TiO2 fibers by combined electrospinning method and hydrothermal reaction. Mater Lett. 2013;106:41-4.
22. You Y, Zhang S, Wan L, Xu D. Preparation of continuous TiO2 fibers by sol–gel method and its photocatalytic degradation on formaldehyde. Appl Surf Sci. 2012;258(8):3469-74.
23. Jiang Z, Gyurova LA, Schlarb AK, Friedrich K, Zhang Z. Study on friction and wear behavior of polyphenylene sulfide composites reinforced by short carbon fibers and sub-micro TiO2 particles. Compos Sci Technol. 2008;68(3–4):734-42.
24. Sundaran SP, Reshmi CR, Sagitha P, Sujith A. Polyurethane nanofibrous membranes decorated with reduced graphene oxide–TiO2 for photocatalytic templates in water purification. J Mater Sci. 2020;55(14):5892-907.
25. Samadi M, Moshfegh AZ. Recent developments of electrospinning-based photocatalysts in degradation of organic pollutants: principles and strategies. ACS Omega. 2022;7(50):45867-81.
26. Wang W, Yang R, Li T, Komarneni S, Liu B. Advances in recyclable and superior photocatalytic fibers: Material, construction, application and future perspective. Compos B Eng. 2021;205:108512.
27. Zhang F, Wang X, Liu H, Liu C, Wan Y, Long Y, et al. Recent advances and applications of semiconductor photocatalytic technology. Appl Sci (Basel). 2019;9(12):2489.
28. Huang ZM, Zhang YZ, Kotaki M, Ramakrishna S. A review on polymer nanofibers by electrospinning and their applications in nanocomposites. Compos Sci Technol. 2003;63(15):2223-53.
29. Mahadadalkar MA, Park N, Yusuf M, Nagappan S, Nallal M, Park KH. Electrospun Fe doped TiO2 fiber photocatalyst for efficient wastewater treatment. Chemosphere. 2023;330:138599.
30. Sigmund W, Yuh J, Park H, Maneeratana V, Pyrgiotakis G, Daga A, et al. Processing and structure relationships in electrospinning of ceramic fiber systems. J Am Ceram Soc. 2006;89(2):395-407.
31. Kumar Sharma G, Rachel James N. Electrospinning: the technique and applications. In: Maaz Khan, Samson Jerold Samuel Chelladuri, editor. Recent developments in nanofibers research. London: IntechOpen; 2023. p. 1-27
32. Al-Abduljabbar A, Farooq I. Electrospun polymer nanofibers: processing, properties, and applications. Polymers (Basel). 2022;15(1):65.
33. Subbiah T, Bhat GS, Tock RW, Parameswaran S, Ramkumar SS. Electrospinning of nanofibers. J Appl Polym Sci. 2005;96(2):557-69.
34. Horner CB, Low K, Nam J. Electrospun scaffolds for cartilage regeneration. In: Liu H, editor. Nanocomposites for musculoskeletal tissue regeneration. Amsterdam: Elsevier; 2016. p. 213-40.
35. Medeiros ES, Glenn GM, Klamczynski AP, Orts WJ, Mattoso LHC. Solution blow spinning: a new method to produce micro- and nanofibers from polymer solutions. J Appl Polym Sci. 2009;113(4):2322-30.
36. Padovani GS, Sanches AO, Moura Aouada MR, Malmonge LF, de Paula FR. Photocatalytic and antimicrobial efficacy of PVDF/TiO2 membranes fabricated by solution blow spinning. J Appl Polym Sci. 2023
37. Silva MJ, Dias YJ, Yarin AL. Electrically-assisted supersonic solution blowing and solution blow spinning of fibrous materials from natural rubber extracted from havea brasilienses. Ind Crops Prod. 2023;192:116101.
38. Carriles J, Nguewa P, González-Gaitano G. Advances in biomedical applications of solution blow spinning. Int J Mol Sci. 2023;24(19):14757.
39. Daristotle JL, Behrens AM, Sandler AD, Kofinas P. A review of the fundamental principles and applications of solution blow spinning. ACS Appl Mater Interfaces. 2016;8(51):34951-63.
40. Chen L, Mei S, Fu K, Zhou J. Spinning the future: the convergence of nanofiber technologies and yarn fabrication. ACS Nano. 2024;18(24):15358-86.
41. Sousa EA, Sanches AO, Vilches JL, da Silva MJ, de Paula FR, McMahan CM, et al. Ribbon-like microfiber of vulcanized and non-vulcanized natural rubber obtained by the solution blow spinning. Polym Adv Technol. 2024;35(2)
42. Zhang X, Wang DK, Lopez DRS, Diniz da Costa JC. Fabrication of nanostructured TiO 2 hollow fiber photocatalytic membrane and application for wastewater treatment. Chem Eng J. 2014;236:314-22.
43. Hoffmann MR, Martin ST, Choi W, Bahnemann DW. Environmental applications of semiconductor photocatalysis. Chem Rev. 1995;95(1):69-96.
44. Fujishima A, Rao TN, Tryk DA. Titanium dioxide photocatalysis. J Photochem Photobiol Photochem Rev. 2000;1(1):1-21.
45. Tan NPB, Cabatingan LK, Lim KJA. Synthesis of TiO2 Nanofiber by Solution Blow Spinning (SBS) Method. Key Eng Mater. 2020;858:122-8.
46. Daristotle JL, Behrens AM, Sandler AD, Kofinas P. A review of the fundamental principles and applications of solution blow spinning. ACS Appl Mater Interfaces. 2016;8(51):34951-63.
47. Bessergenev VG, Mateus MC, do Rego AMB, Hantusch M, Burkel E. An improvement of photocatalytic activity of TiO2 Degussa P25 powder. Appl Catal A Gen. 2015;500:40-50.
48. Kralchevska R, Milanova M, Tsvetkov M, Dimitrov D, Todorovsky D. Influence of gamma-irradiation on the photocatalytic activity of Degussa P25 TiO2. J Mater Sci. 2012;47(12):4936-45.
49. Hanaor DAH, Sorrell CC. Review of the anatase to rutile phase transformation. J Mater Sci. 2011;46(4):855-74.

50. Wang CC, Ying JY. Sol−gel synthesis and hydrothermal processing of anatase and rutile titania nanocrystals. Chem Mater. 1999;11(11):3113-20.
51. Li W, Ni C, Lin H, Huang CP, Shah SI. Size dependence of thermal stability of TiO2 nanoparticles. J Appl Phys. 2004;96(11):6663-8.
52. Choudhury B, Choudhury A. Local structure modification and phase transformation of TiO2 nanoparticles initiated by oxygen defects, grain size, and annealing temperature. Int Nano Lett. 2013;3(1):55.
53. Bizarria MTM, d'Ávila MA, Mei LHI. Non-woven nanofiber chitosan/peo membranes obtained by electrospinning. Braz J Chem Eng. 2014;31(1):57-68.
54. Aydogdu A, Sumnu G, Sahin S. A novel electrospun hydroxypropyl methylcellulose/polyethylene oxide blend nanofibers: morphology and physicochemical properties. Carbohydr Polym. 2018;181:234-46.
55. Pielichowski K, Flejtuch K. Non-oxidative thermal degradation of poly(ethylene oxide): kinetic and thermoanalytical study. J Anal Appl Pyrolysis. 2005;73(1):131-8.
56. Kim BS, Lee J. Macroporous PVDF/TiO2 membranes with three-dimensionally interconnected pore structures produced by directional melt crystallization. Chem Eng J. 2016;301:158-65.
57. Hieu NT, Baik SJ, Chung OH, Park JS. Fabrication and characterization of electrospun carbon nanotubes/titanium dioxide nanofibers used in anodes of dye-sensitized solar cells. Synth Met. 2014;193:125-31.
58. Yuliarto B, Septina W, Fuadi K, Fanani F, Muliani L, Nugraha. Synthesis of nanoporous TiO_2 and its potential applicability for dye-sensitized solar cell using antocyanine black rice. Adv Mater Sci Eng. 2010;2010:1-6.
59. Zhang J, Yan S, Fu L, Wang F, Yuan M, Luo G, et al. Photocatalytic degradation of rhodamine B on anatase, rutile, and brookite TiO2. Chin J Catal. 2011;32(6-8):983-91.
60. Linsebigler AL, Lu G, Yates JT. Photocatalysis on Ti02 surfaces: principles, mechanisms, and selected results. Chem Rev. 1995 [cited 2024 May 22];95(3):735-58. Available from: https://pubs.acs.org/doi/10.1021/cr00035a013
61. Kudo A, Miseki Y. Heterogeneous photocatalyst materials for water splitting. Chem Soc Rev. 2009;38(1):253-78.
62. Odling G, Robertson N. Why is anatase a better photocatalyst than rutile? The importance of free hydroxyl radicals. ChemSusChem. 2015;8(11):1838-40.
63. Luttrell T, Halpegamage S, Tao J, Kramer A, Sutter E, Batzill M. Why is anatase a better photocatalyst than rutile? Model studies on epitaxial TiO2 films. Sci Rep. 2014;4(1):4043.
64. Su R, Bechstein R, Sø L, Vang RT, Sillassen M, Esbjörnsson B, et al. How the anatase-to-rutile ratio influences the photoreactivity of TiO_2. J Phys Chem C. 2011;115(49):24287-92.